

Channel Estimation and Equalization of Zero-Padded Waveforms in Doubly-Dispersive Channels

Javier Lorca Hernando, *Student Member, IEEE*, Lianet Méndez-Monsanto, *Student Member, IEEE*, and Ana García Armada, *Fellow, IEEE*

Abstract—This paper introduces a novel Reference Signal and a channel estimation and equalization technique for Zero-Padded waveforms, like ZP-OFDM and the recently proposed FM-OFDM, under doubly-dispersive channels with Doppler and phase noise. We describe a two-stage pilot structure aimed to separately capture the long-term and short-term channel variations and a piecewise estimation and equalization technique, based on approximation of the time-varying channel impulse response by a set of time-invariant channel responses, which are independently equalized and further combined to compensate the channel's dispersion. Design criteria for the proposed Reference Signal are also given. Numerical results under high phase noise show that piecewise-equalized ZP-OFDM can outperform MMSE-equalized CP-OFDM with CPE compensation, thus avoiding the need of an additional Reference Signal for phase noise mitigation. Results under high mobility demonstrate the superiority of piecewise-equalized FM-OFDM and ZP-OFDM waveforms over MMSE-equalized OTFS and CP-OFDM, outperforming also the highly complex DFE-equalized OTFS for certain modulation orders, without the need to estimate any Doppler components. The degradation incurred by the proposed realistic piecewise estimation technique with respect to ideal estimation depends on the richness of the channel's multipath profile rather than its Doppler spread.

Index Terms—Equalization, Channel estimation, Time-varying channels, Doppler effect, Phase noise.

I. INTRODUCTION

THE Sixth Generation (6G) of wireless cellular communications is already being discussed at the main standardization fora and driven by the studies performed by the International Mobile Telecommunication (IMT) Systems for 2030. One of the key drivers foreseen for 6G is the efficient transmission of wireless signals under strong Doppler conditions, as encountered in, e.g., non-terrestrial networks (NTN) [1]. Another key pillar is the support of extremely high data rates at very high frequencies where phase noise (PN)

is an important factor. The use of Cyclic Prefix-Orthogonal Frequency Division Multiplexing (CP-OFDM) is challenged by its well-known drawbacks, like the high Peak to Average Power Ratio (PAPR) and strong sensitivity to Doppler and PN. Among the new waveform proposals, Orthogonal Time-Frequency-Space (OTFS) modulation is one of the most studied for doubly-dispersive channels based on the delay-doppler representation [2]. Orthogonal chirp division multiplexing (OCDM) [3] and Affine Frequency Division Multiplexing (AFDM) [4] also emerged as new candidates that modulate data onto orthogonal complex chirps to exploit multipath diversity and better cope with doubly dispersive channels, respectively. More recently, Frequency-Modulated Orthogonal Frequency Division Multiplexing (FM-OFDM) was shown to exhibit remarkable resilience to Doppler and PN thanks to differentially encoding the information in the phase and the concept of the *cutoff subcarrier* [5]–[7]. However, most studies rely on perfect channel knowledge by the receiver, and realistic channel estimation in doubly-dispersive conditions demands further research.

Channel estimation based on so-called Basis Expansion Model (BEM) decomposes the time-varying impulse response into a set of pre-defined deterministic functions whose coefficients are to be estimated [8]. BEM models are restrictive in the sets of channels that can be modeled, since they must exhibit properties close to those of the deterministic functions, which hinders adequate modeling of a-priori unknown channels. One popular approach to equalization involves inter-carrier interference (ICI) compensation via Minimum Mean Squared Error (MMSE) equalizers, that exploit the banded structure of the channel matrix either in CP-OFDM or in Zero Padding Orthogonal Frequency Division Multiplexing (ZP-OFDM) [9], [10]. The latter is an appealing alternative to CP-OFDM that ensures symbol recovery regardless of the zero locations of the channel frequency response, and is especially attractive when strong frequency selectivity is present [11], [12]. However, none of these directions provide a fully satisfactory solution, either because of ICI compensation complexity or from a strong dependence on the selected BEM functions, especially when coupled with PN. A more straightforward approach makes use of multi-segmental OFDM equalization with partial Discrete Fourier Transforms (DFTs), where the channel impulse response is approximated by a set of time-varying terms in the so-called piecewise linear model (PLM) [13], [14]. However, equalization of such time-varying impulse

J. Lorca Hernando is with Wireless Labs Europe, InterDigital (e-mail: Javier.LorcaHernando@InterDigital.com). L. Méndez-Monsanto and A. García Armada are with the Department of Signal Theory and Communications, Universidad Carlos III de Madrid, 28911 Leganés, Spain (e-mails: 100384026@alumnos.uc3m.es, agarcia@tsc.uc3m.es).

This work was supported by the CHIST-ERA grant CHIST-ERA-22-WAI-04 through AEI PCI2023-145990-2, by the MCIN/AEI/10.13039/501100011033/ through SOFIA-AIR project (PID2023-147305OB-C31), and partially funded by the European Commission Horizon Europe SNS JU 6G-XR project (GA 101096838). Views and opinions expressed are however those of the author(s) only and do not necessarily reflect those of the European Union. Neither the European Union nor the granting authority can be held responsible for them.

responses cannot be achieved with the traditional techniques devised for time-invariant systems.

In this work, a new channel estimation and equalization technique is introduced for linear time-varying (LTV) channels based on approximation by a set of *piecewise linear time-invariant* (LTI) channel responses, which are readily equalized using *full-interval DFTs*. A suitable two-stage Reference Signal (RS) structure is proposed comprising a Wideband RS (WB-RS) and a Narrowband RS (NB-RS) that are time-interleaved with different periodicities. WB-RS and NB-RS can be separately optimized for estimation of the long-term multipath delays and short-term complex amplitude variations, respectively. While WB-RS resembles the pilots traditionally used for channel estimation (but much sparser in time), NB-RS exhibits two symmetric block structures tailored to track the channel tap variations under known delays.

Estimation relies on the ZP field to approximate the non-circulant Channel Impulse Response (CIR) matrix by a set of circulant CIR matrices. We show that the LTV channel can be locally approximated by a set of piecewise LTI channels, each valid at a different symbol interval, thanks to the trailing zeroes of the ZP field that ensure circularity of the received symbol regardless of the Doppler and PN variations. Obtaining the LTI channels reduces to multiplication of the received signal with a pre-computed pseudo-inverse matrix by relying on the a-priori known tap delays previously estimated with WB-RS. The pseudo-inverse problem can be more conveniently solved using a Tikhonov regularization method when the matrix is ill-conditioned, as happens when the number of pilot subcarriers is small compared to the DFT size. Once the LTI channels are obtained, a piecewise equalization strategy comprises a bank of parallel equalizers for each piecewise interval whose outputs are further combined with window functions.

The main contributions of this paper are summarized as follows:

- A two-stage RS structure is introduced aimed for independent estimation of the channel's multipath delays and complex amplitude variations, respectively, in doubly-dispersive channels with Doppler and PN. Criteria for dimensioning of the proposed RS are given.
- A *realistic piecewise channel estimation technique* is discussed based on decomposition of the LTV channel into multiple piecewise LTI channels, whose responses are obtained by a Tikhonov regularization method. Contrary to other delay-Doppler estimation methods, the Doppler components in our approach do not need to be estimated.
- A *piecewise equalization* strategy initially described in [15] is further elaborated comprising a bank of one-tap equalizers based on full DFTs, each tuned to one of the piecewise LTI channel responses, whose outputs are combined via window functions. The use of partial DFTs is avoided thanks to a remarkable property of Zero-Padded waveforms by which *symbol circularity is preserved regardless of the channel variations*.
- Numerical results illustrate the effectiveness of the proposed approaches with FM-OFDM and ZP-OFDM under high Doppler or high PN conditions. Piecewise equalization at high speeds is remarkably good in FM-OFDM per

its inherent resistance to Doppler, outperforming DFE-equalized OTFS at the higher modulation orders, followed by ZP-OFDM. At high PN conditions, ZP-OFDM outperforms CP-OFDM even when PN compensation is applied to the latter. The effectiveness of real piecewise channel estimation is shown to depend on the multipath profile rather than the amount of Doppler spread, which makes it ideal for high-speed applications.

The rest of the paper is organized as follows. Section II introduces the system model. Section III discusses the approximation of a time-varying channel by a set of time-invariant channel responses in Zero-Padded waveforms. Section IV presents the piecewise channel estimation approach and proposes a suitable RS to accomplish it. Section V details the time-frequency piecewise equalization method based on the piecewise channel approximation. Section VI is devoted to numerical results, and finally Section VII concludes the work.

Notation: $j \triangleq \sqrt{-1}$ is the imaginary unit. For scalars, $\lceil \cdot \rceil$ denotes the rounding to the next higher integer. For a complex vector, $\|\cdot\|$ denotes its norm, $(\cdot)^*$ is the complex conjugate, $(\cdot)^H$ is the Hermitian conjugate, and $\text{vec}(a, b)$ denotes a column vector obtained after vertical stacking of the column vectors a and b . For a complex matrix $\mathbf{A} = \{A_{nm}\}$, its Frobenius norm is denoted by $\|\mathbf{A}\|_F \triangleq \sqrt{\sum_{n,m} |A_{nm}|^2}$. A diagonal matrix with entries A_{nn} at its diagonal is denoted by $\text{diag}(A_{nn})$. N -point vectors are denoted by either $\{b_i, 0 \leq i \leq N-1\}$ or $[b[n], 0 \leq n \leq N-1]$. $\hat{a}[n]$ represents an estimation of $a[n]$. When applied to complex vectors, $a \otimes_N b$ is the N -point linear convolution of a and b , and $a \circledast_N b$ is the N -point circular convolution. The $N \times N$ DFT matrix \mathbf{F}_N is defined by its complex (k, n) -th elements $\frac{1}{\sqrt{N}} \exp(-j2\pi kn/N)$. $\mathbb{E}\{\cdot\}$ represents the expectation operator. $\delta[n]$ is the discrete Dirac delta function. $CN(\eta, \sigma^2)$ is a circularly symmetric complex Gaussian random process with mean η and variance σ^2 .

II. SYSTEM MODEL

The system model considers the transmission of a block of complex modulated symbols using a Zero-Padded waveform over the duration of a symbol. Transmission suffers the impact of a doubly-dispersive channel with delay spread and Doppler spread. A receiver comprising non-ideal oscillators introduces PN impairments over the received signal and is aimed to estimate the original modulated symbols with the best possible error performance.

In every T_s -seconds block interval, a block of N_s complex modulated M -ary Quadrature Amplitude Modulation (M -QAM) symbols $\{X_j\}$ is generated. We assume that T_s can be comparable to, or higher than, the channel's coherence time. For simplicity, we will consider that $\mathbb{E}\{|X_j|^2\} = 1$. The complex modulated symbols are carried by a single-carrier or multi-carrier waveform $p[n]$ characterized by a subcarrier spacing $\text{SCS} = 1/T_s$ and a sampling frequency $f_s = N/T_s$. A mathematical transformation \mathcal{F} then converts the waveform into a different complex baseband signal $\bar{s}[n]$ with possibly better PAPR characteristics than the original waveform, to which a ZP field is appended to the symbol with a length

N_{ZP} equal or higher than the maximum delay of the channel expressed in samples,

$$\begin{aligned} \bar{s}[n] &= \mathcal{F}\{p[n]\}, \\ s[n] &= \begin{cases} \bar{s}[n], & n = 0, \dots, N-1 \\ 0, & n = N, \dots, N+N_{\text{ZP}}-1. \end{cases} \end{aligned} \quad (1)$$

By way of examples, an identity transformation $\mathcal{F} = \mathcal{I}$ would yield a ZP-OFDM waveform, whereas a FM-OFDM waveform with modulation index m and N_a active data subcarriers [7] could be obtained by a transformation (with suitable parameters A_c , θ and φ_0)

$$\mathcal{F}\{p[n]\} = A_c \exp j\{\varphi_t[n] + \theta\}, \quad (2)$$

where $\varphi_t[n] = \varphi_0 + 2\pi \sum_{n'=0}^n f[n']$ and $f[n] = m\sqrt{\frac{N}{N_a}}p[n]$.

The signal $s[n]$ is transmitted over a doubly-dispersive wireless channel that exhibits both delay spread and Doppler spread. A receiver with non-ideal hardware introduces some random PN in addition to Additive White Gaussian Noise (AWGN). Thanks to the appended ZP, linear convolutions become circular convolutions over the padded symbol with length $N_T = N + N_{\text{ZP}}$ irrespective of the time-varying nature of the channel, so the received signal is

$$r[n] = \left(\sum_{z=0}^{N_T-1} h[n, z] s[z] \right) e^{j\varphi_P[n]} + w[n], \quad (3)$$

for $n = 0, \dots, N_T - 1$. $e^{j\varphi_P[n]}$ represents the PN impairment and $w[n]$ is $\mathcal{CN}(0, N_0)$ where N_0 is the one-sided noise spectral density.

Thanks to the signal's circularity, one-tap frequency-domain equalization can undo multipath with the aid of the channel's impulse response obtained via channel estimation. Note that channel estimation in time-varying channels should consider the *intra-symbol channel variations* caused by Doppler and PN. Finally, the inverse of the transformation performed by the transmitter is applied to the equalized signal $\hat{r}[n]$ to obtain an estimate of the original waveform $\hat{p}[n] = \mathcal{F}^{-1}\{\hat{r}[n]\}$, from which the estimated complex modulated symbols $\{\hat{X}_j\}$ can be obtained.

A. Transmitter

A block diagram is shown in Fig. 1 illustrating the processing steps for block-based transmission and reception of a Zero-Padded waveform. Over the duration of a symbol, a QAM modulator delivers a block of N_s complex modulated M -QAM symbols $\{X_j\}$. The modulated symbols are then mapped to subcarriers via the vector $X[k]$. The waveform-specific transformation \mathcal{F} in (1) can be suitably decomposed into a pre-DFT step (that yields $X_{\text{pre}}[k]$) and a post-DFT step (that yields $f_{\text{post}}[n]$), between which a normalized N -point IDFT converts the frequency-domain information $X_{\text{pre}}[k]$ into the time-domain signal vector $f[n]$. A ZP field of length N_{ZP} is finally appended to deliver the transmitted signal vector $s[n]$ with length $N_T \triangleq N + N_{\text{ZP}}$.

Different pre-DFT and post-DFT steps can yield different waveforms. For example, ZP-DFT-s-OFDM can be obtained with a transform precoding pre-DFT stage and no post-DFT

step; FM-OFDM results from a frequency modulation post-DFT step and no pre-DFT step [7]; and ZP-OFDM involves no pre-DFT or post-DFT steps [11].

B. Channel Model

A doubly-dispersive LTV channel exhibiting delay spread and Doppler spread is assumed [16], [17] that further belongs to the broad set of *parsimonious* channel models [18], a subclass of so-called underspread channels characterized by a limited Doppler spread. Embedding the PN contribution of (3) as part of the LTV channel response $h[n, z]$, the discrete-time input-output representation can be written as a convolution-like operation,

$$r[n] = \sum_{z=0}^{N_T-1} h[n, z] s[n-z] + w[n], \quad (4)$$

where $s[n]$ and $r[n]$ are the transmitted and received signal vectors respectively, $h[n, z]$ is the *time-varying impulse response* of the channel, and $w[n]$ is the complex Gaussian noise term. $h[n, z]$ is a function of the discrete delay z and discrete time n and exhibits smooth temporal variations per as the limited Doppler and PN impairment. Virtually all realistic radio channels are underspread [18], and the combined frequency impairment from Doppler and PN is smaller than one subcarrier spacing in most terrestrial applications [7]. For a given delay z_0 , the time-varying functions $h[n, z_0]$ are commonly known as channel taps and can each be attributed to a macroscopic scatterer. Although it is customary to consider uncorrelated scatterers, this work does not rely on that assumption.

In its simplest form, parsimonious channels can be described by a tapped delay line with L time-varying channel taps $\{b_l[n]\}_{l=0, \dots, L-1}$, where the path delay of the channel taps can be resolved into a set of discrete delays $z_l = \lfloor \tau_l f_s \rfloor$ corresponding to the continuous-time delays τ_l ,

$$h[n, z] = \sum_{l=0}^{L-1} b_l[n] \delta[z - z_l]. \quad (5)$$

Notice that $b_l[n]$ may contain additional time-varying effects from, e.g., PN caused by oscillators, thus rendering $h[n, z]$ an effective time-varying channel impulse response (CIR) as seen by the receiver. This channel model can correspond to either pure non-line of sight (NLOS) dominated by Rayleigh scattering, or line-of-sight (LOS) with a direct ray and some Rayleigh fading caused by scatterers. Large-scale fading is not considered as it runs over time scales of seconds to minutes (much larger than the symbol duration N_T) depending on the environment, and only small-scale fading is assumed to have an impact on performance [17].

C. Receiver

The time-varying channel response $h[n, z]$ must be estimated and equalized prior to demodulation. Instead of carrying out a BEM decomposition of the channel, we develop an extension of the *partitioned convolutions* technique proposed in [19] and adapt it for use in parsimonious channels, by

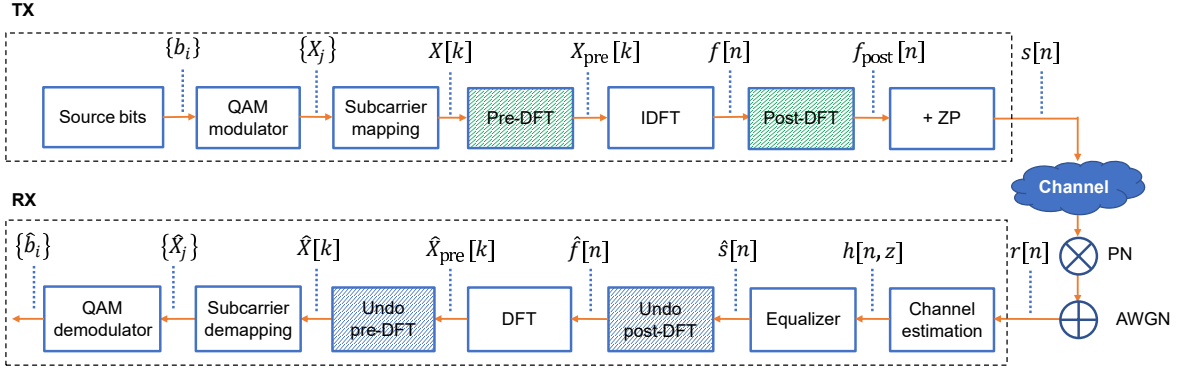


Fig. 1. Block diagram for block-based transmission and reception of a Zero-Padded waveform over a doubly-dispersive channel subject to AWGN and PN. Unshaded blocks are common to ZP-OFDM, while different shaded blocks lead to different waveforms.

which $b_l[n]$ are approximated by a set of step functions in the variable n (Section III). Contrary to the approach in [13], [14] where the weighted outputs of several partial interval DFTs are linearly combined, our equalization strategy performs full-interval DFTs whose windowed outputs are combined to yield the signal vector $\hat{s}[n]$ (Section V). Full-interval DFTs are beneficial for implementations because of their lower complexity, $O(N \log N)$, compared to partial-interval DFTs, $O(N \log^2 N)$ [20].

After undoing any pre/post-DFT processing steps in Fig. 1 and performing an N -point DFT, the signal vector $\hat{X}[k]$ contains the estimated subcarrier contents $X[k]$. The Subcarrier demapping block finally picks the N_s subcarriers containing the received M -QAM symbols $\{\hat{X}_j\}$.

III. APPROXIMATION OF LTV CHANNELS BY TIME-INVARIANT CHANNEL RESPONSES

A. CIR Matrix Approximation

Let us examine the input-output relationship (4),

$$\mathbf{R} = \mathbf{H}\mathbf{S} + \mathbf{W}, \quad (6)$$

where $\mathbf{R} = [r[n]]^T$ is the N_T -point received signal vector, $\mathbf{S} = [s[n]]^T$ is the N_T -point Zero-Padded transmitted symbol, $\mathbf{H} \in \mathbb{C}^{N_T \times N_T}$ is the CIR matrix, and $\mathbf{W} = [w[n]]^T$ is the N_T -point noise. Let us assume a generic CIR with length $L = N_{\text{ZP}}$ and $z_l = l$. The CIR matrix is then

$$\mathbf{H} = \begin{bmatrix} b_0[0] & 0 & 0 & \cdots & b_1[0] \\ b_1[1] & \ddots & \vdots & & \vdots \\ \vdots & & 0 & \cdots & b_{L-1}[L-2] \\ b_{L-1}[L-1] & \cdots & b_0[N_T-L] & \cdots & 0 \\ 0 & \ddots & b_1[N_T-L+1] & \ddots & \vdots \\ \vdots & & \vdots & & 0 \\ 0 & \cdots & b_{L-1}[N_T-1] & \cdots & b_0[N_T-1] \end{bmatrix}. \quad (7)$$

Notice that the non-null upper terms of the $L-1$ last columns have no impact on the result, because they multiply the N_{ZP} zeroes in the ZP field. They could be set to zero, which makes

\mathbf{H} a lower triangular matrix whose effect on the input signal reduces to a linear combination of up to $L-1$ previous samples weighted by the channel coefficients, with no effect from the signal or the channel at other time instants. We call this the *locality property enabled by ZP*.

Leveraging the smoothness of the time-varying taps $b_l[n]$ in (5), we assume that their variations can be approximated by a set of N_L step functions whose constant complex amplitudes are obtained by sampling $b_l[n]$ at the time instants $(2i+1)\Delta/2$, where $\Delta = N/N_L$ is the length of each step function. This, combined with the locality property enabled by ZP, allows us to approximate the effect of the LTV channel at each interval $n \in \Delta_i$ (including PN) by

$$h[n, z] \simeq h_i[z], \quad \forall n \in [0, N-1] : i\Delta \leq n < (i+1)\Delta, \quad (8)$$

where $\{h_i[z], i \in [0, N_L-1]\}$ are obtained by sampling $h[n, z]$ at $n = (2i+1)\Delta/2$,

$$h_i[z] \triangleq h[(2i+1)\Delta/2, z] = \sum_{l=0}^{L-1} b_{i,l} \delta[z - z_l], \quad (9)$$

with $b_{i,l} \triangleq b_l[(2i+1)\Delta/2]$. The LTI impulse response $h_i[z]$ in (9) has a circulant CIR matrix $\mathbf{H}_i \in \mathbb{C}^{N_T \times N_T}$ equal to the matrix that describes the implicit circular convolution operation,

$$\mathbf{H}_i = \begin{bmatrix} b_{i,0} & 0 & 0 & \cdots & b_{i,L-1} \\ b_{i,1} & \ddots & \vdots & & \vdots \\ \vdots & & 0 & \cdots & b_{i,L-1} \\ b_{i,L-1} & \cdots & b_{i,0} & \cdots & 0 \\ 0 & \ddots & b_{i,1} & \ddots & \vdots \\ \vdots & & \vdots & & 0 \\ 0 & \cdots & b_{i,L-1} & \cdots & b_{i,0} \end{bmatrix}. \quad (10)$$

Notice that \mathbf{H}_i has dimensions $N_T \times N_T$ and is thus defined over the whole symbol. Therefore, the channel output can be locally approximated by the output of its corresponding piecewise-constant LTI channel at the intervals $n \in \Delta_i$,

$$\mathbf{R} \simeq \mathbf{H}_i \mathbf{S} + \mathbf{W}, \quad n \in \Delta_i : i \in [0, N_L-1], \quad (11)$$

or, in vector form,

$$r[n] \simeq h_i[n] \otimes_{N_T} s[n] + w[n], \quad n \in \Delta_i : i \in [0, N_L-1]. \quad (12)$$

In conclusion, when the CIR matrix is obtained over the N_T points including ZP, the LTV channel can be locally approximated by a set of LTI channels because ZP preserves circularity regardless of the Doppler and PN variations [11]. Intuitively, the trailing zeroes of the ZP field ensure that the received symbols comprise circularly-shifted replicas of the input signal regardless of the channel variations. This contrasts with the case of a CP pre-pended to the symbols, like in CP-OFDM, where time variations make the CIR matrix no longer circulant [10].

B. Piecewise Approximation Error

The rms error incurred by replacing the LTV channel with a set of piecewise LTI channels can be obtained from the ICI power that remains after the piecewise approximation. For a Doppler spread f_D and symbol duration T_s , the ICI power P_{ICI} is bounded by the universal upper bound $P_{ICI} \leq \frac{1}{3} (\pi f_D T_s)^2$ valid for any Doppler spectra [21]. This upper bound can be modified to account for a PN linewidth W_{PN} [22] in addition to the Doppler spread, since their multiplicative effects lead to added spectral widths because of the implicit convolution. After splitting the symbol into N_L intervals, the rms piecewise approximation error over a duration given by the piecewise interval (T_s/N_L) plus the channel's delay spread ($\sim 1/B_c$, where B_c is the channel's coherence bandwidth) becomes

$$\varepsilon_{LTI} \leq \frac{\pi (f_D + W_{PN})}{\sqrt{3}} \left(\frac{T_s}{N_L} + \frac{1}{B_c} \right). \quad (13)$$

The first term inside the brackets usually dominates over the delay spread, which leads to the rms error in [15] when no PN is present. This upper bound can be useful for a-priori dimensioning of the value N_L needed to meet a target ε_{LTI} , under worst-case values of the Doppler spread f_D , PN linewidth W_{PN} , and channel's delay spread $1/B_c$. However, it disregards any impact from imperfect channel estimation.

IV. PIECEWISE ESTIMATION OF LTV CHANNELS

With the insight gained in Section III, we now introduce a strategy to estimate the N_L CIR responses $h_i[n]$ based on a suitable RS structure for Zero-Padded waveforms.

A. Proposed RS Structure

A two-stage RS structure is proposed as shown in Fig. 2 comprising a combination of Wideband RS (WB-RS) and Narrowband RS (NB-RS) signals that are time-interleaved as in the figure. The receiver can leverage both to estimate the complex amplitudes $b_{i,l}$ and delays z_l in (9) prior to equalization.

WB-RS is aimed to estimate the multipath delays z_l with a time resolution determined by the allocated bandwidth $B_u = N_u/T_s$. Its structure is similar to a traditional RS for channel estimation, but it comprises N_W consecutive symbols for improved SNR in the delay estimation and exhibits a *longer repetition period* T_d as per the much slower variations expected for the channel delays. T_d can be upper bounded by the time needed for a multipath delay to change by one

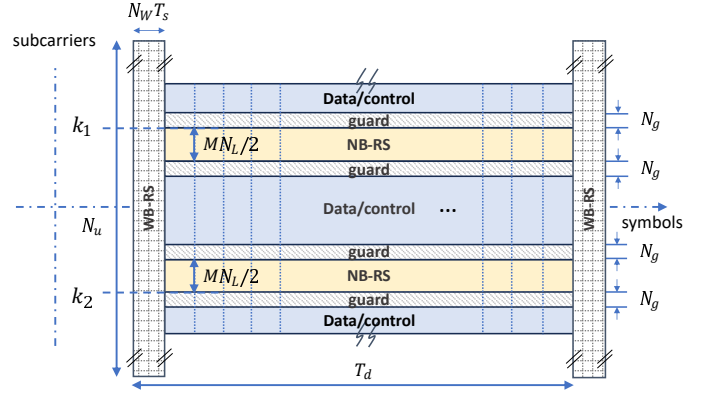


Fig. 2. Proposed two-stage RS for LTV channel estimation comprising WB-RS and NB-RS signals that are mapped in frequency and time-interleaved with a certain periodicity. In ZP-OFDM, four guard bands of N_g subcarriers each are reserved to separate NB-RS from other allocated subcarriers. In FM-OFDM, N_g can be set to zero.

sample as a result of the user's movement. For a velocity v and sampling frequency f_s , the time needed for the receiver to traverse the same distance as the light covers in the duration of a sample is $c/(f_s v)$. Relating it with the channel's coherence time $T_c \sim 1/f_D = c/(f_c v)$,

$$T_d \lesssim \frac{c}{f_s v} = \frac{f_c}{f_s} T_c, \quad (14)$$

and the WB-RS period can be orders of magnitude longer than the channel's coherence time.

NB-RS is aimed to track the time-varying complex tap amplitudes $b_{i,l}$. It is constructed from a complex sequence \mathbf{C} with length MN_L ($M \in \mathbb{N}$) that is mapped to the contiguous subcarriers of two symmetric blocks at both sides of the carrier center, each of size $MN_L/2$, with indices

$$\mathcal{K} = \{k_1, \dots, k_1 + MN_L/2 - 1, k_2 - MN_L/2 + 1, \dots, k_2\},$$

where $k_1, k_2 \in [0, N_u - 1]$. The block structure of NB-RS allows capturing the intra-symbol channel variations required by the piecewise approximation. Mapping NB-RS away from the carrier center ensures that the time-domain pilot signal undergoes wider variations from the higher-order subcarriers involved, which leads to a lower Cramer-Rao Bound (CRB) of the estimation error from the lower value of the second-order derivative in the Fisher information matrix [23], [24]. In high-Doppler or high PN scenarios, NB-RS should be present in every symbol, otherwise its repetition period can be set equal or lower than T_c .

In ZP-OFDM, four guard bands of N_g subcarriers each are reserved to isolate NB-RS from any adjacent data/control subcarriers allocated in the same symbol. Its role is to minimize the degradation in channel estimation caused by ICI from the adjacent data/control part. For a Doppler spread f_D and PN linewidth W_{PN} , an obvious criterion leads to

$$N_g \gtrsim \left\lceil \frac{f_D + W_{PN}}{\text{SCS}} \right\rceil. \quad (15)$$

In contrast, the FM-OFDM spectral response exhibits significant tails at the edges of the system bandwidth because of

the angular modulation, and the N_T subcarriers have non-zero power [7]. Hence, pilots must be superimposed with some of the original subcarriers, N_g can be set to zero, and interference must be accounted for in the demodulation process. Allocating the pilots in an intermediate region between the carrier center and the edges can reduce their impact while keeping control of the spectral leakage towards adjacent channels.

In what follows, N_a denotes the number of subcarriers carrying payload data. In ZP-OFDM, both payload and pilots are mapped to non-overlapping sets of subcarriers in the frequency domain. In FM-OFDM, payload is mapped to the instantaneous frequency spectrum [7].

Taking into account that $T_d \gg T_s$ by several orders of magnitude, the contribution from WB-RS to the RS overhead η_{RS} can be neglected and we can write

$$\eta_{RS} = \frac{N_u}{N} \frac{N_W T_s}{T_d} + \frac{MN_L + 4N_g}{N} \left(1 - \frac{N_W T_s}{T_d}\right) \simeq \frac{MN_L + 4N_g}{N}, \quad (16)$$

or, when $N_g = 0$ like in FM-OFDM,

$$\eta_{RS} \simeq \frac{MN_L}{N}. \quad (17)$$

Incorporating this into the spectral efficiencies of ZP-OFDM and FM-OFDM [7] (respectively ϵ_{ZP} and ϵ_{FM}), we can write

$$\begin{aligned} \epsilon_{ZP} &\simeq K_{QAM} \frac{MN_L + 4N_g}{N}, \\ \epsilon_{FM} &\simeq \frac{N_a K_{QAM}}{4T_s \left(mf_s + \frac{N_a}{2T_s}\right)} \frac{MN_L}{N}. \end{aligned} \quad (18)$$

As will be seen in Section VI, reasonable results are obtained with an RS overhead between 25% and 50% for ETSI Highway NLOS and 3GPP TDL-C channel models, respectively. In NR, a 50% overhead is characteristic of the so-called DM-RS Configuration Type 1, typical of single-antenna scenarios [25]. The need to allocate NB-RS in every symbol appears only when the channel's coherence time T_c is comparable to the symbol duration T_s , as assumed throughout this work; otherwise, NB-RS can have the same periodicity as DM-RS and N_L can be equal to 1.

B. Piecewise Channel Estimation

Let us assume a received signal vector $\mathbf{R} \in \mathbb{C}^{N_T \times 1}$ containing both NB-RS and data that passes through an LTV channel, as shown in Fig. 1. The goal of the receiver is to estimate the channel over the subcarriers allocated to the user. An overlap-and-add (OLA) operation is first applied on \mathbf{R} to make the symbol circular by adding the ZP field to the first N_{ZP} samples, as in ZP-OFDM-OLA transceivers [11], yielding a vector

$$\mathbf{R}_{OLA} = \mathbf{R}_u + [\mathbf{R}_l \mathbf{0}_{1 \times (N - N_{ZP})}]^T \in \mathbb{C}^{N \times 1}, \quad (19)$$

where \mathbf{R}_u and \mathbf{R}_l are column vectors containing the upper N rows (indexes 0 to $N - 1$) and the lower N_{ZP} rows (indexes $N_T - N_{ZP}$ to $N_{ZP} - 1$) of \mathbf{R} , respectively. OLA yields an N -point circular vector whose control/data subcarriers can be nulled prior to channel estimation to yield

$$\tilde{\mathbf{R}}_{OLA} = \mathbf{F}_N^H \mathbf{\Pi} \mathbf{F}_N \mathbf{R}_{OLA} \in \mathbb{C}^{N \times 1}. \quad (20)$$

The diagonal matrix $\mathbf{\Pi} = \{\pi_{jk}\} \in \mathbb{C}^{N \times N}$ filters out the subcarriers other than NB-RS as follows,

$$\pi_{jk} = \begin{cases} 1, & (j, k) : j = k \in \mathcal{K} \\ 0, & \text{elsewhere.} \end{cases} \quad (21)$$

Leveraging the piecewise channel approximation, we can now build a matrix equation describing the effect of the channel on the transmitted time-domain NB-RS signal vector. Assuming that the receiver knows the length L of the channel (in number of samples)¹, a matrix equation

$$\tilde{\mathbf{R}}_{OLA} = \mathbf{S}_{OLA} \mathbf{B} \quad (22)$$

can be constructed, where $\mathbf{B} \in \mathbb{C}^{N_L \times 1}$ and $\mathbf{S}_{OLA} \in \mathbb{C}^{N \times N_L}$ are defined by

$$\begin{aligned} \mathbf{B} &= [b_{0,0} b_{0,1} \dots b_{0,L-1} \dots b_{N_L-1,0} b_{N_L-1,1} \dots b_{N_L-1,L-1}]^T, \\ \mathbf{S}_{OLA} &= \begin{bmatrix} \mathbf{V}_0 & \mathbf{0} & \dots & \mathbf{U}_0 \\ \mathbf{U}_1 & \mathbf{V}_1 & & \vdots \\ \vdots & \ddots & \ddots & \mathbf{0} \\ \mathbf{0} & \dots & \mathbf{U}_{N_L-1} & \mathbf{V}_{N_L-1} \end{bmatrix}, \end{aligned}$$

and $\mathbf{V}_i \in \mathbb{C}^{\Delta \times L}$, $\mathbf{U}_i \in \mathbb{C}^{\Delta \times L}$, $i = 0, \dots, N_L - 1$ are matrices defined by

$$\begin{aligned} \mathbf{V}_i &= \begin{bmatrix} s_{(i\Delta)} & 0 & \dots & 0 & 0 \\ s_{(i\Delta+1)} & s_{(i\Delta)} & \dots & \vdots & \vdots \\ \vdots & \vdots & \ddots & 0 & 0 \\ s_{(i\Delta+L-1)} & s_{(i\Delta+L-2)} & \dots & s_{(i\Delta)} & 0 \\ s_{(i\Delta+L)} & s_{(i\Delta+L-1)} & \dots & s_{(i\Delta+1)} & s_{(i\Delta)} \\ \vdots & \vdots & & \vdots & \vdots \\ s_{((i+1)\Delta-1)} & s_{((i+1)\Delta-2)} & \dots & s_{((i+1)\Delta-L+1)} & s_{((i+1)\Delta-L)} \end{bmatrix}, \\ \mathbf{U}_i &= \begin{bmatrix} 0 & s_{(i\Delta-1) \bmod N} & \dots & s_{(i\Delta-L+1) \bmod N} \\ 0 & 0 & \ddots & \vdots \\ \vdots & \vdots & & s_{(i\Delta-1) \bmod N} \\ 0 & 0 & \dots & 0 \\ \vdots & \vdots & & \vdots \\ 0 & 0 & \dots & 0 \end{bmatrix}. \end{aligned}$$

The terms $s_{(n)}$ in \mathbf{V}_i and \mathbf{U}_i are the elements of the N -point time-domain NB-RS signal vector $\mathbf{C}_N = [s_{(0)} \dots s_{(N-1)}]^T$ constructed from the complex sequence \mathbf{C} by means of

$$\mathbf{C}_N = \mathbf{F}_N^H \text{vec}(\mathbf{C}, \mathbf{0}_{(N-MN_L) \times 1}), \quad (23)$$

where $\mathbf{0}_{p \times 1}$ is a column vector with p zeroes. Notice that, when $N_L = 1$, \mathbf{S}_{OLA} collapses into a circulant matrix equal to the sum of \mathbf{V}_0 and \mathbf{U}_0 .

The Least Squares (LS) Estimator that solves (22) is the vector $\tilde{\mathbf{B}} = \{\tilde{b}_{i,l}\}$ that satisfies

$$\tilde{b}_{i,l} = \arg \min \|\tilde{\mathbf{R}}_{OLA} - \mathbf{S}_{OLA} \tilde{\mathbf{B}}\|_F^2, \quad (24)$$

¹ L can be derived as the sample above which the relative magnitude of the channel response obtained from WB-RS with respect to the maximum is lower than a threshold, e.g., -20 dB. Alternatively, if the delay spread of the channel $\tau_{rms} \sim 1/B_c$ is known, L can be given by $L = \tau_{rms} f_s \simeq \frac{f_s}{B_c}$.

TABLE I
COMPLEXITY AND MEMORY USAGE COMPARISON OF LS AND REAL
PIECEWISE ESTIMATION.

| Estimation | Relative complexity | Memory usage |
|----------------|--|---|
| LS | $N \log N + N_a$ | $2N_b N$ |
| Real piecewise | $2N \log N + NN_L L$ $+ (N + N_{ZP}) \log (N + N_{ZP})$ | $2N_b [N + N_L LN$ $+ N_L (N + N_{ZP})]$ |

subject to the condition $1/N_L \sum_{i=0}^{N_L-1} \sum_{l=0}^{L-1} |\tilde{b}_{i,l}|^2 = P$, where P is the channel's instantaneous power. The solution involves computing the Moore-Penrose pseudo-inverse $(\mathbf{S}_{OLA})^+$,

$$\tilde{\mathbf{B}} = (\mathbf{S}_{OLA})^+ \tilde{\mathbf{R}}_{OLA}, \quad (25)$$

further discarding the elements of $\tilde{\mathbf{B}}$ that are a-priori known to be null with the aid of WB-RS. Calculation of the pseudo-inverse may be challenging if the matrix \mathbf{S}_{OLA} is ill-conditioned. In this case, a Tikhonov regularization method is used to solve the problem as given by [26]

$$\tilde{b}_{i,l} = \arg \min \left\{ \|\tilde{\mathbf{R}}_{OLA} - \mathbf{S}_{OLA} \tilde{\mathbf{B}}\|_F^2 + \lambda^2 \|\tilde{\mathbf{B}}\|_F^2 \right\}, \quad (26)$$

where the so-called ridge parameter λ is a-priori known (Section VI-C), with solution

$$\tilde{\mathbf{B}} = \left(\mathbf{S}_{OLA}^H \mathbf{S}_{OLA} + \lambda^2 \mathbf{I} \right)^{-1} \mathbf{S}_{OLA}^H \tilde{\mathbf{R}}_{OLA}. \quad (27)$$

As will be seen in Section V, equalization requires knowledge of the frequency responses of the N_L LTI channels over the whole symbol length including ZP. This can be computed via N_T -point DFTs of the sub-vectors $\tilde{\mathbf{B}}_i$, $i = 0, \dots, N_L - 1$, formed by extraction of the rows iL to $iL + L - 1$ from $\tilde{\mathbf{B}}$, leading to

$$\tilde{\mathbf{H}}_i = \mathbf{F}_{N_T} \text{vec}(\tilde{\mathbf{B}}_i, \mathbf{0}_{(N_T-L) \times 1}) \in \mathbb{C}^{N_T \times 1}. \quad (28)$$

C. Estimation Complexity and Memory Usage

Complexity can be calculated as the number of floating-point multiplications per symbol neglecting any other processing steps. Taking into account that (19) does not involve any such multiplication, and that both the pseudo-inverse matrix $(\mathbf{S}_{OLA})^+$ in (25) and the terms that multiply $\tilde{\mathbf{R}}_{OLA}$ in (27) can be pre-computed for known values of L , N_L and λ , the piecewise estimation complexity is shown in Table I and compared with a traditional LS estimation. It is to note that N dominates over N_{ZP} in most practical systems, which leads to a piecewise estimation complexity roughly equal to $3N \log N + NN_L L$.

The overhead from storing the pre-computed terms in (27) can be quantified by comparing the memory usage in both algorithms, also shown in Table I. For a binary representation with N_b bits per floating-point sample, LS estimation requires storage of a single N -point complex vector for the frequency response, whereas piecewise estimation requires an additional complex matrix of size $(N_L L \times N)$ plus N_L complex vectors of length N_T points for the LTI frequency responses.

D. Piecewise Estimation Error

The Normalized Mean Squared Error NMSE incurred in the estimation can be obtained from

$$\text{NMSE} = \frac{\|\tilde{\mathbf{R}}_{OLA} - \mathbf{S}_{OLA} \tilde{\mathbf{B}}\|_F^2}{\|\tilde{\mathbf{R}}_{OLA}\|_F^2}. \quad (29)$$

Note that NMSE already accounts for the thermal noise power and the error incurred by the piecewise channel approximation ε_{LTI} in (13) over the N_L intervals. In the case of ideal piecewise channel estimation, $\tilde{\mathbf{B}}$ equals \mathbf{B} .

E. Extension to Multi-Antenna Systems

The two-stage RS structure can be extended to support systems comprising multiple antennas. Without loss of generality, the different antenna ports can be associated with distinct WB-RS/NB-RS pairs to enable unambiguous estimation of their corresponding time-varying channel responses. WB-RS can thus follow a staggered frequency allocation of resources for antenna port multiplexing, whereas NB-RS can be mapped to non-overlapping subcarrier positions. If $MN_L/2$ is smaller than the channel's coherence bandwidth (expressed in number of subcarriers), multiple NB-RS can be code-division multiplexed in the same subcarriers to incur minimal resources consumption, e.g., via multiplication with orthogonal Walsh-Hadamard codes [25].

V. PIECEWISE EQUALIZATION IN ZERO-PADDED WAVEFORMS

Assuming knowledge of the LTI channel responses, the next task of the receiver is to undo their effect in order to recover the information conveyed by the transmitted signal.

A. Time-Frequency Equalization of LTV Channels

We now focus on the CIR matrices \mathbf{H}_i in (10). \mathbf{H}_i is a circulant matrix that allows diagonalization via post(pre) multiplication by $N_T \times N_T$ -point (I)DFT matrices [11]. Moreover, the locality property enabled by ZP allows to locally equalize the signal at the intervals $n \in \Delta_i$ and suitably combine the results [15]. Equation (12) suggests an equalization strategy that comprises a bank of N_L parallel equalizers applied to the received signal $r[n]$ whose outputs are combined to yield $\hat{s}[n]$, as shown in Fig. 3. Exploiting the circulant property of the CIR matrices \mathbf{H}_i , estimates of the transmitted signal $\hat{\mathbf{S}}_i$ can be obtained from

$$\hat{\mathbf{S}}_i = \mathbf{F}_{N_T}^H \mathbf{M}_i \mathbf{F}_{N_T} \mathbf{R}, \quad 0 \leq i \leq N_L - 1, \quad (30)$$

where $\mathbf{M}_i \triangleq \text{diag}(M_{i,k})$, $k \in [0, N_T - 1]$ is an equalizer's diagonal matrix aimed to undo the effect of the i -th LTI channel. As an example, the transfer function

$$M_{i,k} = \frac{\tilde{H}_{i,k}^*}{|\tilde{H}_{i,k}|^2 + N_{\text{eff}}}, \quad k \in [0, N_T - 1], \quad (31)$$

characterizes a linear MMSE equalizer where the i -th estimated channel's frequency response $\tilde{\mathbf{H}}_i \triangleq \{\tilde{H}_{i,k}\}$ is given by (28). The term N_{eff} in (31) must account for both thermal noise

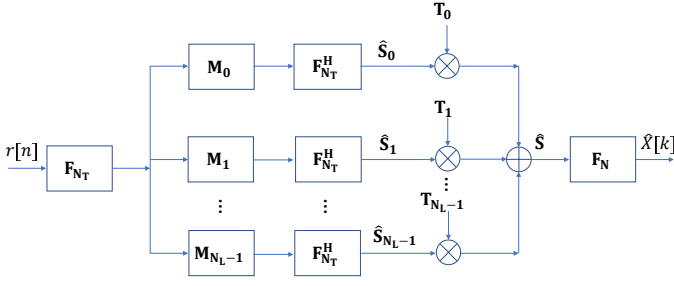


Fig. 3. Block diagram of a piecewise equalizer comprising a bank of N_L one-tap equalizers aimed to compensate the LTI channels, whose outputs are further combined via window functions.

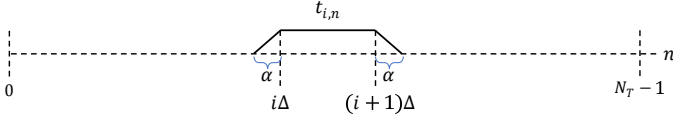


Fig. 4. Trapezoidal window function $t_{i,n}$ defined at the i -th interval with an overlap with the adjacent intervals controlled by α .

and the incurred piecewise approximation error $\varepsilon_{\text{LTI}}^2$. N_{eff} can be upper bounded by (see (13))

$$N_{\text{eff}} = N_0 + \varepsilon_{\text{LTI}}^2 \leq N_0 + \frac{1}{3} \left[\pi (f_D + W_{\text{PN}}) \left(\frac{T_s}{N_L} + \frac{1}{B_c} \right) \right]^2. \quad (32)$$

Thanks to the locality property enabled by ZP, the equalized signals $\hat{\mathbf{S}}_i$ from (30) are valid estimations of \mathbf{S} at the intervals $n \in \Delta_i$. Therefore, by defining N_L window matrices

$$\mathbf{T}_i \triangleq \text{diag}(t_{i,n}), \quad n \in [0, N_T - 1], \quad (33)$$

whose diagonal entries $t_{i,n}$ are non-null mainly at the intervals $n \in \Delta_i$ under the condition that $\sum_i t_{i,n} = 1 \quad \forall n \in [0, N - 1]$, we can construct the N_T -point equalized signal vector as

$$\hat{\mathbf{S}} = \sum_{i=0}^{N_L-1} \{ \mathbf{T}_i \mathbf{F}_{N_T}^H \mathbf{M}_i \} \mathbf{F}_{N_T} \mathbf{R}. \quad (34)$$

Finally, the estimated subcarrier contents $\hat{X}[k]$ in Fig. 1, neglecting any pre-DFT or post-DFT steps, can be obtained by application of an N -point DFT to the estimated symbol $\hat{\mathbf{S}}$.

The window matrices \mathbf{T}_i can be arbitrarily defined as long as their non-null values are mainly concentrated at the intervals $n \in \Delta_i$ and their accumulated sum renders unity. Discontinuities at the boundaries can be alleviated by partially allowing window functions to spill over the adjacent intervals, under the control of a roll-off parameter $\alpha \in \mathbb{N}$. The simplest case involves a set of trapezoidal functions as in Fig. 4,

$$t_{i,n} = \begin{cases} \frac{n-i\Delta}{\alpha} + 1, & i\Delta - \alpha \leq n < i\Delta \\ 1, & i\Delta \leq n < (i+1)\Delta \\ \frac{(i+1)\Delta - n}{\alpha} + 1, & (i+1)\Delta \leq n < (i+1)\Delta + \alpha \\ 0, & \text{elsewhere} \end{cases} \quad (35)$$

Another suitable option is the finite-length normalized Raised Cosine window with roll-off parameter $0 \leq \beta \leq 1$, as shown in Fig. 5 for a duration of $2N_L$ symbols with an oversampling factor equal to Δ .

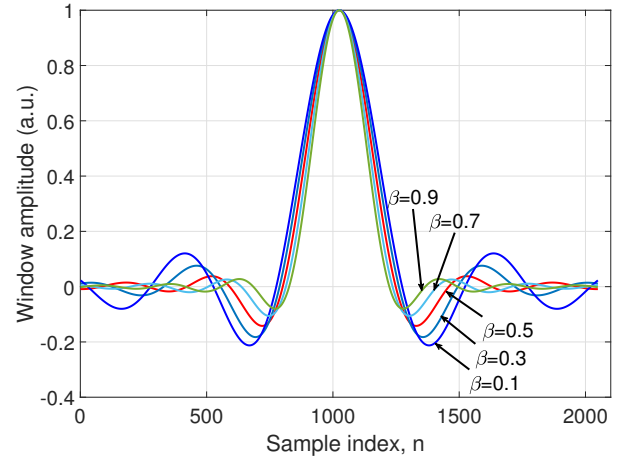


Fig. 5. Finite-length normalized Raised Cosine window function $t_{i,n}$ spanning $2N_L = 8$ symbols with oversampling factor $\Delta = 256$, plotted as a function of the roll-off parameter β .

TABLE II
COMPLEXITY AND MEMORY USAGE COMPARISON OF MMSE AND PIECEWISE MMSE EQUALIZATION.

| Equalization | Relative complexity | Memory usage |
|----------------|--|-------------------|
| MMSE | $3N_a$ | $2N_b N$ |
| Piecewise MMSE | $(N_L + 1)(N + N_{\text{ZP}}) \log(N + N_{\text{ZP}}) + N_L(4N + 3N_{\text{ZP}}) + N \log N$ | $2N_b(N + N_L N)$ |

B. Equalization Complexity, Memory Usage and Latency

Considering a bank of MMSE equalizers as in Fig. 3, Table II compares the piecewise MMSE equalization complexity with that of traditional MMSE equalization, assuming prior knowledge of the N_L LTI channels. Piecewise equalization exhibits an increased complexity that is, however, largely outweighed by its benefits under high mobility or high PN, as shown in what follows. The memory usages in MMSE and piecewise MMSE are also compared, the main difference lying in the need to store N_L window functions of length N with the latter (which can however be significantly reduced due to the sparsity of the windows).

It is worth also quantifying the latency differences in both schemes. Given its parallel structure, piecewise equalization has a relative added latency of two DFT steps (with matrices $\mathbf{F}_{N_T}^H$ and \mathbf{F}_N respectively) plus a complex multiplication with the window \mathbf{T}_i . The latter can be very fast given the sparsity of most practical window functions, while FFTs can benefit from efficient implementations of the Cooley-Tukey algorithm. However, the presence of two DFT sizes (N and N_T) calls for an extra optimization when sizes cannot be factored by powers of 2, 3 and 5 [27], since FFT implementations are usually optimized for those sizes.

VI. NUMERICAL RESULTS

In this section, theoretical expressions are numerically verified and the bit error rate (BER) performance is assessed for ZP-OFDM and FM-OFDM, further comparing them with CP-OFDM and OTFS. Numerical results in AWGN (with PN) and high-Doppler Rayleigh fading channels (without PN)

TABLE III
SIMULATION ASSUMPTIONS.

| Parameter | Value |
|---------------------------------|--|
| Carrier frequency, f_c | 4 GHz and 30 GHz |
| DFT length, N | 1024 |
| No. data subcarriers, N_a | 128, 256, 384, 512, and 600 |
| Subcarrier spacing, SCS | 15 kHz and 120 kHz |
| Channel types | AWGN, 3GPP TDL-C (300) [28], 3GPP NTN-TDL-A (100) [29], and ETSI Highway NLOS [30] |
| Doppler spectrum | Classical Jakes in all taps |
| User speed, v | 30-2000 km/h (no PN), 0 km/h (PN) |
| PN model | 3GPP mmWave SSB model [31] |
| PT-RS density | $L_{PT-RS} = 1$, $K_{PT-RS} = 2$ (CP-OFDM) |
| FM-OFDM parameters | $m_{FM} = 0.6/2\pi$ to $0.8/2\pi$; $k_0 = 0$ |
| Frame structure | NR-like with 14 symbols per slot |
| Modulation | QPSK, 16QAM, 64QAM, 256QAM |
| Channel Estimation | Ideal ($M = 0$) and Real piecewise ($M > 0$) |
| No. guard subcarriers, N_g | 1 for Real piecewise estimation in ZP-OFDM, 0 otherwise |
| NB-RS sequence C | Based on $N_L = 4$ concatenated Zadoff-Chu sequences with root indexes 2, 4, 5, and 8, cyclically-extended up to length $M = 32$ or 64 |
| NB-RS allocation (k_1, k_2) | $k_1 = 101$, $k_2 = 924$ (with DC subcarrier at 512) |
| WB-RS allocation | $N_W = 4$ symbols every 99 slots spanning full bandwidth (11.1 MHz) |
| DM-RS configuration | Mapping Type A, Configuration Type 1, with 3 additional positions [25] |
| Equalization | MMSE (CP-OFDM and OTFS), piecewise MMSE (ZP/FM-OFDM), and DFE (OTFS) |
| Number of intervals, N_L | 2, 4, 8, and 16 |
| Window functions, $t_l[n]$ | Trapezoidal with $\alpha = 0$ Raised Cosine with β between 0.1 and 0.9 |

are presented under both ideal piecewise and real piecewise channel estimation conditions, and the estimation NMSE is compared with the theoretical piecewise estimation error in the latter case. The simulation assumptions are summarized in Table III. In all plots, SNR reflects the signal-to-noise ratio averaged over the whole symbol considering the CP/ZP field, the value of N_a , and any NB-RS signal inserted for piecewise channel estimation (if applicable).

A. Equalization Performance under High Mobility - Ideal Piecewise Estimation

The bit error rate performance of piecewise equalization is numerically assessed assuming ideal piecewise approximation, in which the estimated channel responses $\hat{\mathbf{H}}_i$ in (28) are equal to the elements of the CIR matrix \mathbf{H}_i in (10).

Firstly, an analysis of the impact of the window function on the equalization performance is shown in Fig. 6 for both trapezoidal and Raised Cosine function types, with different values of β in the latter case. It is apparent that differences between both are negligible, as explained by their similar energy concentration at the interval centers and relative decay at both edges. In what follows, only trapezoidal windows are considered for simplicity when obtaining numerical results.

Fig. 7 and Fig. 8 show the impact of N_L on the ZP-OFDM performance with 3GPP TDL-C (300) channel model at 120 km/h and 500 km/h with no PN. Increasing N_L

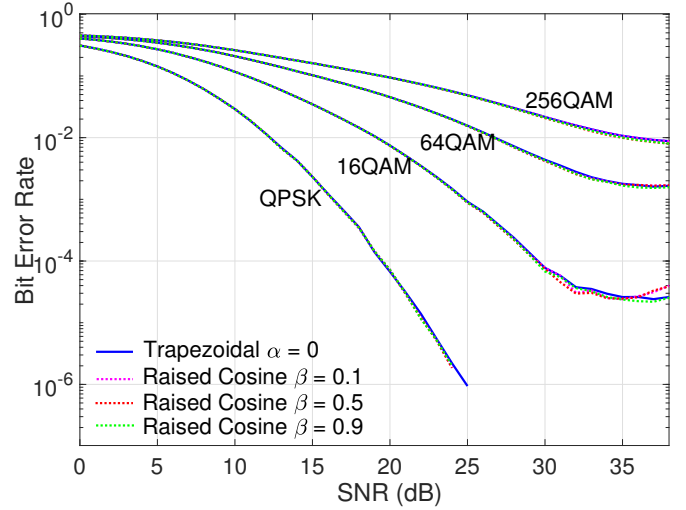


Fig. 6. Impact of the window function on the bit error rate performance of piecewise-equalized FM-OFDM in TDL-C (300) channel at 120 km/h, with SCS = 15 kHz, $N_L = 4$, $N_a = 600$, $f_c = 4$ GHz, $m_{FM} = 0.8/2\pi$ (QPSK) and $m_{FM} = 0.7/2\pi$ (16/64/256QAM).

pushes the error floor down to a minimum achieved with $N_L = 4$ (120 km/h) or $N_L = 8$ (500 km/h), above which it becomes detrimental because of the higher impact of border effects. In QPSK, nearly optimum performance is obtained with $N_L = 2/4$ (120/500 km/h). The unexpected degradation observed in Fig. 8 above the optimum SNR for high N_L is caused by the higher prevalence of residual ICI errors at high SNR, under which MMSE equalization becomes less effective despite the lower overall noise level. In addition to that, an error floor appears at higher SNR because of (30), which is aimed to separately undo the effects of multipath at each of the N_L intervals. Doing so amounts to re-aligning and coherently combining the received time-domain signal replicas. This operation can involve samples from adjacent intervals, possibly affected by channel tap values that are different to those in the current interval, leading to residual tap variations. The resulting performance depends on the waveform resilience to such variations, which is higher in FM-OFDM thanks to differentially encoding the information in the instantaneous frequency [7].

Fig. 9 illustrates the behavior of FM-OFDM, OTFS and CP-OFDM with TDL-C (300) channel at 120 km/h. OTFS curves are obtained with both MMSE equalizer and Decision Feedback Equalizer (DFE) [2], [32], while FM-OFDM considers piecewise MMSE equalization and $N_L = 4$. Whereas CP-OFDM is barely usable at this speed, FM-OFDM performance is close to OTFS-MMSE in QPSK, stays between OTFS-MMSE and OTFS-DFE in 16QAM, and is remarkably better than the highly complex OTFS-DFE in 64/256QAM. Notice that FM-OFDM has slightly worse performance than OTFS or CP-OFDM below the threshold SNR (10 dB) because of the use of linear equalization, but quickly improves above it. This is caused by the higher likelihood of phase unwrap errors when close to the threshold, and can be mitigated by so-called threshold extension techniques [33] or the use of detectors avoiding phase demodulators [34], [35]. OTFS-MMSE and

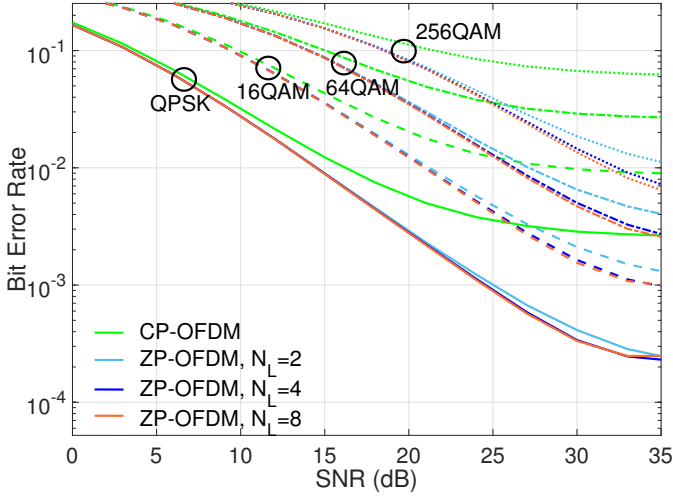


Fig. 7. Impact of N_L on the bit error rate performance of CP-OFDM and piecewise-equalized ZP-OFDM in TDL-C (300) channel at 120 km/h, with SCS = 15 kHz, $N_a = 600$, and $f_c = 4$ GHz.

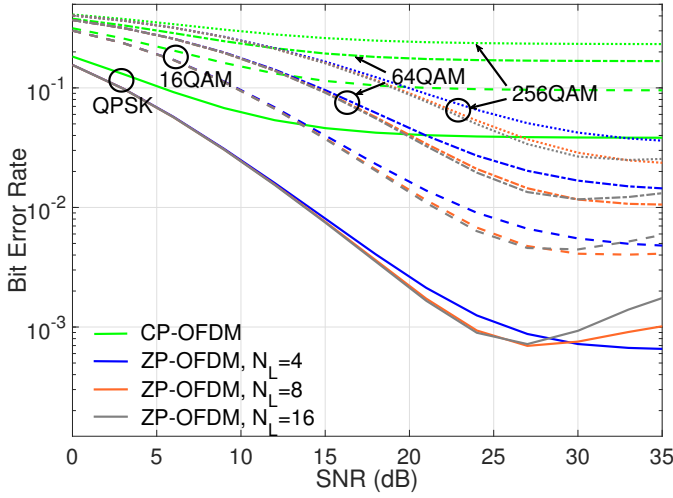


Fig. 8. Impact of N_L on the bit error rate performance of CP-OFDM and piecewise-equalized ZP-OFDM in TDL-C (300) channel at 500 km/h, with SCS = 15 kHz, $N_a = 600$, and $f_c = 4$ GHz.

FM-OFDM exhibit similar degradation as ZP-OFDM above their optimal SNR points because of the lower effectiveness of MMSE equalization under mobility [32].

It is insightful to illustrate the impact of the N/N_a ratio on the piecewise-equalized FM-OFDM performance by examining the case with $N_a = 128$ in Fig. 10. FM-OFDM here exhibits steeper BER curves and better diversity than in Fig. 9. A higher value of N/N_a achieves less phase unwrap errors and better spreading of the data in the time domain when modulating the instantaneous frequency, because differentially encoding the information in the phase differences yields better protection at the lower instantaneous frequency subcarriers thanks to the $1 - \cos()$ noise shape [7]. Moreover, the error floor is significantly reduced, showing asymptotic values that are below 10^{-5} in 64QAM and below 10^{-4} in 256QAM. This excellent performance comes at the cost of a lower spectral efficiency (from the lower value of N_a) because the

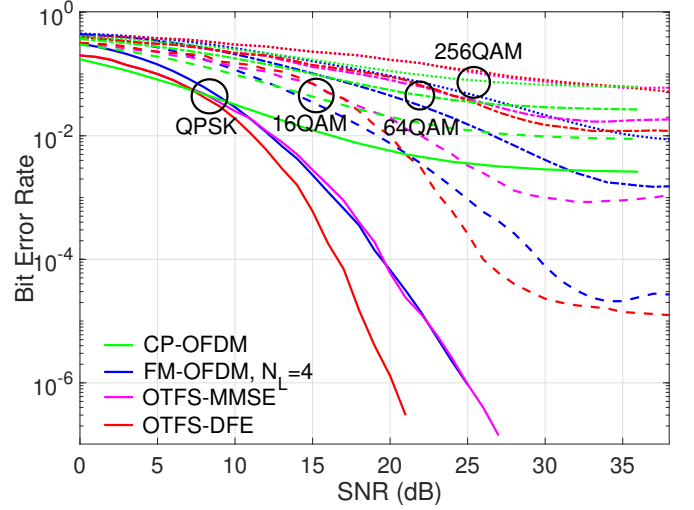


Fig. 9. Bit error rate comparison between piecewise-equalized FM-OFDM, OTFS, and CP-OFDM waveforms in TDL-C (300) channel at 120 km/h, with SCS = 15 kHz, $N_a = 600$, $f_c = 4$ GHz, $m_{FM} = 0.8/2\pi$ in QPSK and $m_{FM} = 0.7/2\pi$ in 16/64/256QAM.

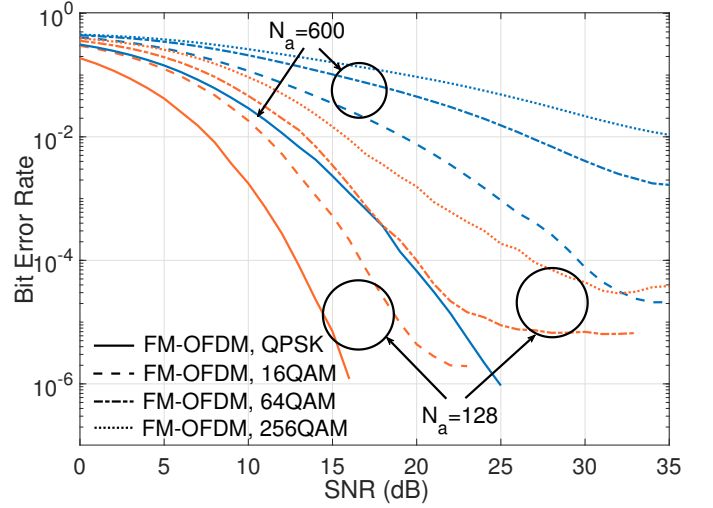


Fig. 10. Bit error rate comparison of piecewise-equalized FM-OFDM waveform for two values of N_a in TDL-C (300) channel at 120 km/h, with SCS = 15 kHz, $f_c = 4$ GHz, $N_L = 4$, $m_{FM} = 0.7/2\pi$ (QPSK) and $m_{FM} = 0.6/2\pi$ (16/64/256QAM).

bandwidth reduction is not commensurate with the reduction in N_a for a given modulation index [7]. Increasing m similarly improves performance, but degrades spectral efficiency up to an optimum m beyond which phase errors start to dominate. This trade-off between performance and spectral efficiency is a remarkable characteristic of FM-OFDM inherited from angular modulations, further strengthened by its unique robustness to Doppler and PN.

The relative insensitivity of piecewise-equalized FM-OFDM to Doppler is illustrated in the curves of Fig. 11. FM-OFDM effectively spreads the information in both frequency (from the FM modulation) and time (from the IDFT in Fig. 1). Moreover, residual equalizer errors are additive, and mostly confined within the subcarrier interval $k \in [-k_0, k_0]$ at the instantaneous frequency spectrum, thus posing a lesser threat

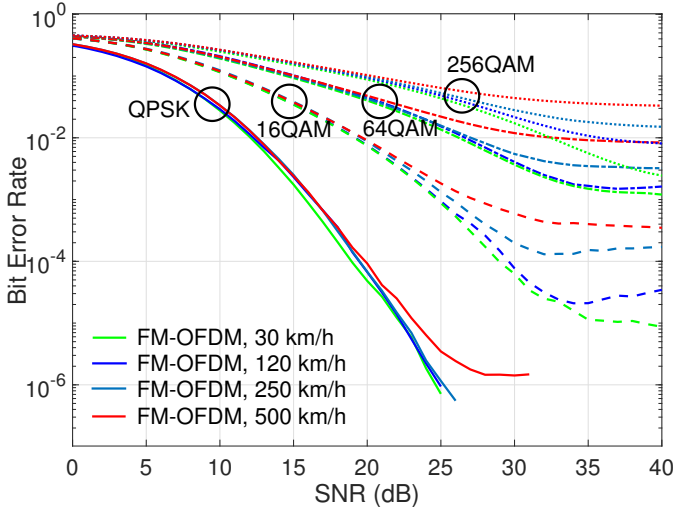


Fig. 11. Bit error rate performance of piecewise-equalized FM-OFDM in TDL-C (300) channel at 30, 120, 250 and 500 km/h, with SCS = 15 kHz, $N_a = 600$, $f_c = 4$ GHz, $N_L = 4$, $m_{FM} = 0.8/2\pi$ (QPSK) and $m_{FM} = 0.7/2\pi$ (16/64/256QAM).

to the signal [7]. These relatively stable channel conditions in FM-OFDM caused by spreading is what the authors in [36] denote by “equal gain criterion”, and is proven to maximize performance under very general receiver conditions. Contrary to OTFS, stability of the channel is achieved without spreading the information over multiple time-domain symbols, with an important benefit on latency.

The more stringent Doppler conditions in Fig. 12 correspond to a NTN-TDL-A (100) channel up to 2000 km/h. This is a worst-case NLOS scenario that does not consider the relatively smaller Doppler shifts encountered in practice in most NTN scenarios, e.g., when receiving a beam from a LEO satellite [37]. CP-OFDM is essentially unusable at these speeds, and thus only piecewise-equalized FM-OFDM and ZP-OFDM are shown with $N_L = 8$. FM-OFDM performs remarkably well and is quite insensitive to speed up to 1000 km/h, with noticeable degradation only at 2000 km/h. The cutoff subcarrier k_0 is deliberately set to zero and can always be optimized in this case to better absorb impairments, especially at the higher modulation orders [7]. ZP-OFDM underperforms FM-OFDM and suffers from a much more significant error floor. Despite this, piecewise-equalized ZP-OFDM still shows better behavior than any of the banded approaches in the serial and block MMSE equalizers described in [9], as also happens with the TDL-C (100) channel of Fig. 8, and is only behind the non-banded block MMSE approach (deemed impractical since it relies on good estimation of the Doppler components outside the channel matrix band [9]).

B. Equalization Performance under High PN - Ideal Piecewise Estimation

Fig. 13 shows the impact of N_L on a piecewise-equalized ZP-OFDM waveform under AWGN, subject to PN as described in the model of [31], for 16QAM and 64QAM, $f_c = 30$ GHz, and SCS = 120 kHz. CP-OFDM curves are presented with and without common phase error (CPE) compensation

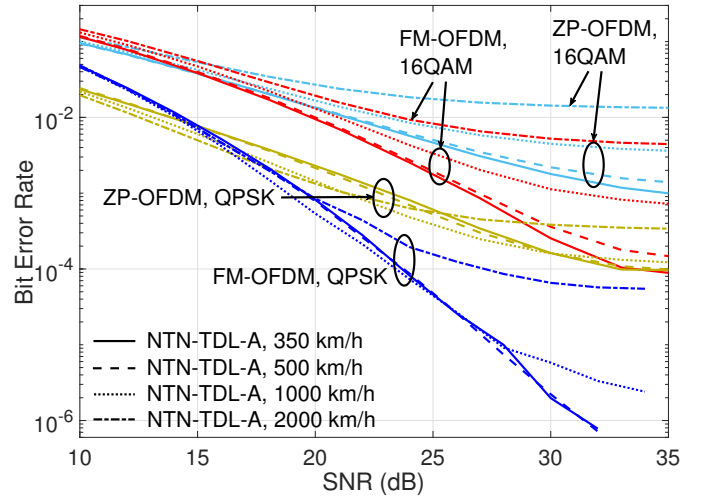


Fig. 12. Impact of speed on piecewise-equalized FM-OFDM and ZP-OFDM waveforms in NTN-TDL-A (100) channel conditions at 350, 500, 1000, and 2000 km/h, with SCS = 15 kHz, $N_a = 600$, $f_c = 4$ GHz, $N_L = 8$, $k_0 = 0$, $m_{FM} = 0.7/2\pi$, and QPSK and 16QAM modulations.

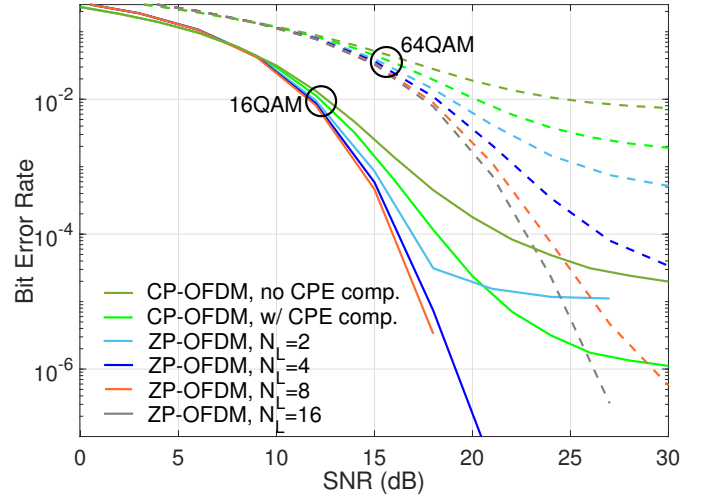


Fig. 13. Impact of N_L on the bit error rate performance of piecewise-equalized ZP-OFDM in AWGN channel with PN, and comparison with CP-OFDM with and without CPE compensation, for 16/64QAM at $f_c = 30$ GHz, $N_a = 600$, SCS = 120 kHz.

as achieved with the aid of an NR PT-RS signal with a periodicity of 1 symbol ($L_{PT-RS} = 1$) and 2 resource blocks ($K_{PT-RS} = 2$) [25]. It is apparent that piecewise-equalized ZP-OFDM outperforms CP-OFDM with CPE compensation for $N_L \geq 2$ (16QAM) and $N_L \geq 4$ (64QAM), thus avoiding the need of an additional RS for phase noise tracking and compensation.

In the presence of PN, the degree of performance control enabled by varying N/N_a in FM-OFDM is nicely illustrated in the numerical results of Fig. 14 and Fig. 15. Notice that, for FM-OFDM, no channel estimation or CPE compensation is needed because PN is equivalent to a flat-fading Rayleigh channel, to which FM-OFDM is remarkably resilient [7]. Piecewise-equalized ZP-OFDM with $N_L = 4$, CPE-compensated CP-OFDM, and OTFS without equalization or CPE compensation are also shown for comparison. Whereas

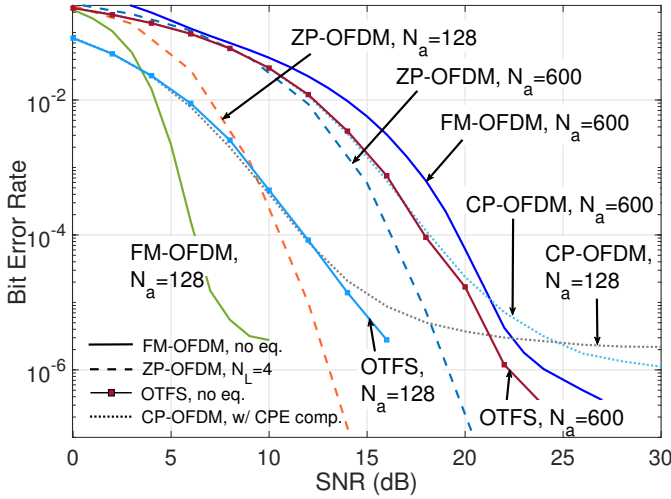


Fig. 14. Bit error rate comparison between FM-OFDM, ZP-OFDM, CP-OFDM, and OTFS for two values of N_a in AWGN channel with PN, for 16QAM, SCS = 120 kHz, and $f_c = 30$ GHz. Piecewise equalization is considered in ZP-OFDM with $N_L = 4$, CP-OFDM includes CPE compensation, while FM-OFDM and OTFS have no channel estimation or CPE compensation.

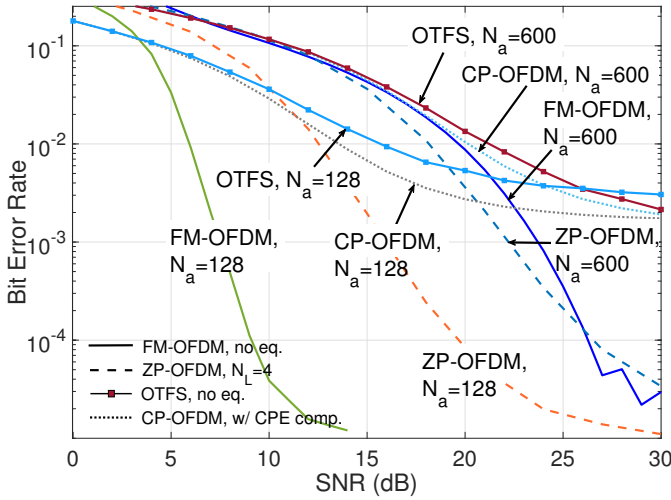


Fig. 15. Bit error rate comparison between FM-OFDM, ZP-OFDM, CP-OFDM, and OTFS for two values of N_a in AWGN channel with PN, for 64QAM, SCS = 120 kHz, and $f_c = 30$ GHz. Piecewise equalization is considered in ZP-OFDM with $N_L = 4$, CP-OFDM includes CPE compensation, while FM-OFDM and OTFS have no channel estimation or CPE compensation.

reducing N_a in ZP-OFDM, CP-OFDM and OTFS simply brings an SNR gain equal to the relative reduction in the number of active subcarriers (~ 6.7 dB), the gain is much more significant in FM-OFDM (~ 14 dB for 16QAM and ~ 17 dB for 64QAM) thanks to the higher protection against PN achieved with increased values of N/N_a , as in the high Doppler case. With $N_a = 600$, FM-OFDM is slightly behind OTFS in 16QAM, but outperforms it in 64QAM, as also observed in Fig. 9. With $N_a = 128$, FM-OFDM outperforms all the others.

C. Equalization Performance under High Mobility - Real Piecewise Estimation

In this subsection, the multipath delays z_l are assumed to be estimated by leveraging the presence of WB-RS transmissions comprising $N_W = 4$ dedicated symbols with a repetition period T_d . For a fair comparison, the WB-RS bandwidth in both ZP-OFDM and FM-OFDM waveforms is set equal to the rms bandwidth of the latter. Errors in delay estimation are accounted for by adding a Gaussian error term to the ideal channel delays at every WB-RS occasion, with a variance equal to the square of the CRB given by $1/(B_{\text{rms}}\sqrt{\text{SNR}})$ [38]. Delays are then rounded to their nearest integer values and used by NB-RS for real piecewise channel estimation until the next transmission of WB-RS.

NB-RS is inserted as shown in Fig. 2 to enable piecewise estimation of $b_{i,l}$, with $N_L = 4$ and a power equal to a fraction MN_L/N_a relative to the power of the data part. The NB-RS location k_1, k_2 are selected so that the power level of the affected data subcarriers in FM-OFDM is at most 20 dB below the peak, avoiding the carrier edges to prevent excessive out-of-band power leakage. No attempt was made to optimize k_1, k_2 but simply show one feasible option. Interference from superimposed NB-RS in FM-OFDM is assumed to be ideally compensated at the receiver by means of a Successive Interference Cancellation (SIC) technique [39]. Results are compared with those obtained from ideal piecewise channel estimation with $N_a = 512$ to maintain the same signal bandwidth.

The pseudo-inverse matrix problem in (25) can be ill-conditioned when the elements of the matrices \mathbf{V}_i and \mathbf{U}_i exhibit low time-domain variations, which happens when $MN_L/N \ll 1$ in (23). As a result, \mathbf{S}_{OLA} exhibits a high condition number and the pseudo-inverse problem is prone to noise amplification. To overcome this issue, a Tikhonov regularization method is used in (26) with $\lambda^2 = N_0$ [26]. The condition number improves with higher values of MN_L .

A comparison between the bit error rate of FM-OFDM and ZP-OFDM with both ideal piecewise and real piecewise channel estimation is shown in Fig. 16 for 16QAM and 64QAM, TDL-C (300) channel, and 300 km/h. With this configuration, the WB-RS bandwidth is 11.1 MHz and the repetition period is 99 slots. Here, $M = 64$ and $N_a = 256$, thus yielding 50% NB-RS overhead as commonly encountered in some NR DM-RS configurations. The performance of MMSE-equalized CP-OFDM is also shown for convenience with both ideal and LS estimation based on DM-RS with 3 additional positions [25]. Real piecewise estimation incurs an SNR degradation of approximately 5-6 dB at a BER of 10^{-1} , and an increase in the error floor, due to the complex multipath profile of TDL-C (24 taps). ZP-OFDM and FM-OFDM with real piecewise estimation intersect at an SNR ≈ 15 -16 dB given by the sum of the threshold SNR for angular modulations [7] (10 dB) and the degradation incurred by real piecewise estimation (≈ 5 -6 dB). The use of threshold extension techniques can be very useful to reduce this crossing SNR [33]. Beyond it, FM-OFDM and ZP-OFDM outperform CP-OFDM. By comparison, Fig. 17 shows the bit error rate performance in ETSI Highway NLOS channel for QPSK and 16QAM, $M = 32$ and $N_a = 384$, and

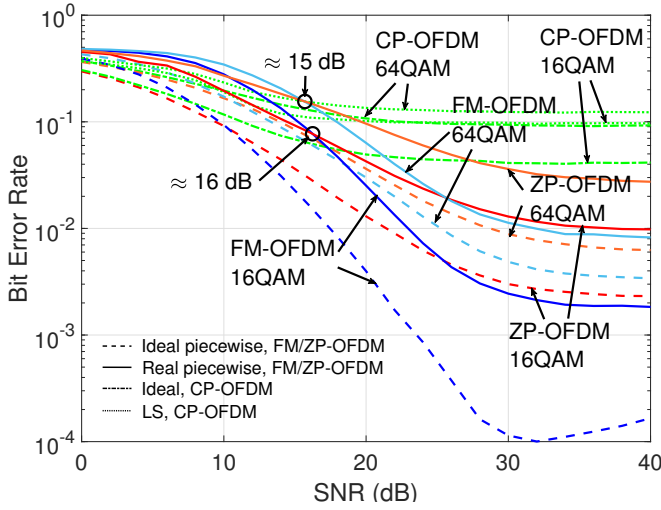


Fig. 16. Bit error rate of piecewise-equalized FM-OFDM and ZP-OFDM, and MMSE-equalized CP-OFDM, under different channel estimation techniques in a TDL-C (300) channel at 300 km/h for 16QAM and 64QAM. SCS = 15 kHz, $f_c = 4$ GHz, $m_{FM} = 0.7/2\pi$, $N_L = 4$, $M = 64$, $N_a = 512$ (ideal and ideal piecewise) and 256 (LS and real piecewise).

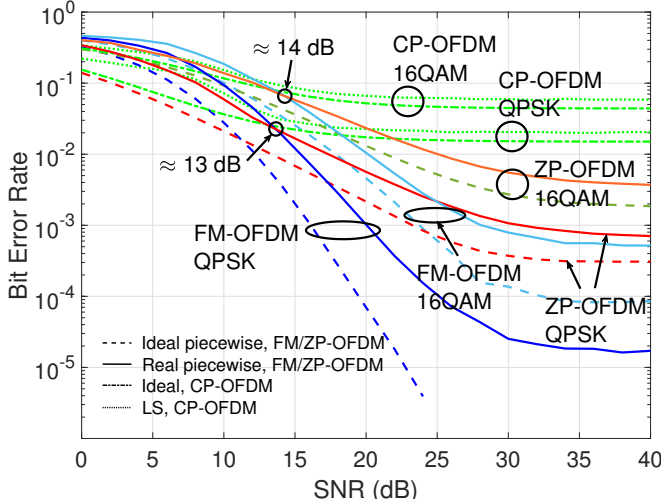


Fig. 17. Bit error rate of piecewise-equalized FM-OFDM and ZP-OFDM, and MMSE-equalized CP-OFDM, under different channel estimation techniques in ETSI Highway NLOS channel at 300 km/h for QPSK and 16QAM. SCS = 15 kHz, $f_c = 4$ GHz, $m_{FM} = 0.7/2\pi$, $N_L = 4$, $M = 32$, $N_a = 512$ (ideal and ideal piecewise) and 384 (LS and real piecewise).

25% NB-RS overhead. The SNR degradation is in this case 3-4 dB at a BER of 10^{-1} despite the lower NB-RS size, as explained by the milder multipath profile in this channel (4 taps) compared to TDL-C.

Fig. 18 depicts the NMSE in (29) obtained from real piecewise estimation in TDL-C (300) and ETSI Highway NLOS channels at 120 km/h and 300 km/h. The squared error bound (13) is also shown for both channels. Since most part of the NMSE is above (13), it is apparent that NMSE is dominated by the imperfections in channel estimation rather than the piecewise approximation error, which justifies the applicability of the piecewise approach. Our NMSE at 300 km/h, or 1111 Hz Doppler spread (9.2×10^{-4} and 1.4×10^{-3} for TDL-C and Highway NLOS channels, respectively), exhibits a

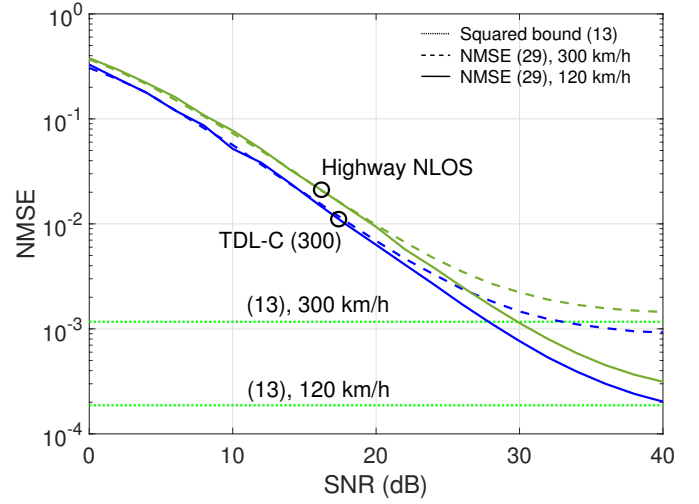


Fig. 18. Normalized Mean Squared Error (29) and squared bound (13) obtained with real piecewise estimation in TDL-C (300) and ETSI Highway NLOS channels at 120 km/h and 300 km/h, for $N_L = 4$ and $M = 64$ (TDL-C) or $M = 32$ (Highway NLOS).

lower irreducible error floor than the five BEM models studied in [40] at ~ 963 Hz Doppler spread (above 2×10^{-3} in all the cases), despite the lack of optimization in the NB-RS symbols or their location.

VII. CONCLUSIONS

In this paper, a channel estimation and equalization technique for Zero-Padded waveforms under strong Doppler and PN is proposed and analyzed. A two-stage RS is introduced to separately derive the LTV channel's delays and complex amplitudes by approximation with a set of piecewise LTI responses, leveraging the locality property enabled by ZP. The RS can be mapped to some of the unused subcarriers, or superimposed with them, in a frequency region comprising two symmetric blocks between the carrier's center and the edges whose location can be further optimized for best spectral leakage-performance tradeoff. Estimation reduces to a Tikhonov regularization problem aimed to reduce the condition number of a pseudo-inverse matrix. A bank of one-tap equalizers using full DFTs is proposed to remove delay dispersion, while Doppler dispersion is effectively mitigated by the piecewise channel approach without having to estimate any Doppler components. Numerical results at high mobility demonstrate the superiority of piecewise-equalized ZP waveforms with ideal piecewise channel estimation, especially FM-OFDM, outperforming DFE-equalized OTFS at 120 km/h and 64QAM/256QAM. Piecewise-equalized ZP-OFDM under high PN significantly outperforms CPE-compensated CP-OFDM without the need of an additional PT-RS-like signal. Finally, realistic piecewise estimation shows reasonable results even if no attempt was made to optimize the RS symbols or their location, with an overhead that depends on the multipath profile and the amount of Doppler.

REFERENCES

- [1] "Future technology trends of terrestrial International Mobile Telecommunications systems towards 2030 and beyond," ITU-R, Technical Report ITU-R M.2516-0, 2022.
- [2] R. Hadani, S. Rakib, M. Tsatsanis, A. Monk, A. J. Goldsmith, A. F. Molisch, and R. Calderbank, "Orthogonal Time Frequency Space Modulation," in *2017 IEEE Wireless Communications and Networking Conference (WCNC)*, 2017.
- [3] X. Ouyang and J. Zhao, "Orthogonal Chirp Division Multiplexing," *IEEE Transactions on Communications*, vol. 64, no. 9, pp. 3946–3957, 2016.
- [4] A. Bemani, G. Cuzzo, N. Ksairi, and M. Kountouris, "Affine Frequency Division Multiplexing for Next-Generation Wireless Networks," in *2021 17th International Symposium on Wireless Communication Systems (ISWCS)*, 2021, pp. 1–6.
- [5] J. Lorca Hernando, "A method to generate a wireless waveform for use in a wireless communication system, a wireless communication system and computer program products thereof," Patent EP3 264 702B1, 2016.
- [6] J. Lorca Hernando and C. González Sánchez, "A method to provide increased robustness against noise and interference in wireless communications, a transmitter and computer program products thereof," Patent EP3 439 255B1, 2017.
- [7] J. Lorca Hernando and A. G. Armada, "Frequency-Modulated OFDM: A New Waveform for High-Mobility Wireless Communications," *IEEE Transactions on Communications*, vol. 71, no. 1, pp. 540–552, 2023.
- [8] G. Giannakis and C. Tepedelenioglu, "Basis expansion models and diversity techniques for blind identification and equalization of time-varying channels," *Proceedings of the IEEE*, vol. 86, no. 10, pp. 1969–1986, 1998.
- [9] L. Rugini, P. Banelli, and G. Leus, "Simple equalization of time-varying channels for OFDM," *IEEE Communications Letters*, vol. 9, no. 7, pp. 619–621, 2005.
- [10] D. Shimbo, N. Maeda, H. Mishima, and J. Ido, "Inter-Carrier Interference Compensation for Zero Padding OFDM," in *2013 IEEE 78th Vehicular Technology Conference (VTC Fall)*, 2013, pp. 1–5.
- [11] B. Muquet, Z. Wang, G. Giannakis, M. de Courville, and P. Duhamel, "Cyclic prefixing or zero padding for wireless multicarrier transmissions?" *IEEE Transactions on Communications*, vol. 50, no. 12, pp. 2136–2148, 2002.
- [12] N. Wang and S. D. Blostein, "Adaptive zero-padding OFDM over frequency-selective multipath channels," *EURASIP Journal on Advanced Signal Processing*, vol. 2004:10, p. 1478–1488, 2004.
- [13] L. A. Li, H. Wei, Y. Yao, G. Chen, W. Ling, J. Du, and Y. Huang, "Multi-segmental OFDM signals equalization with piecewise linear channel model over rapidly time-varying channels," *EURASIP Journal on Wireless Communications and Networking*, vol. 2017:191, 2017.
- [14] S. Yerramalli, M. Stojanovic, and U. Mitra, "Partial FFT Demodulation: A Detection Method for Highly Doppler Distorted OFDM Systems," *IEEE Transactions on Signal Processing*, vol. 60, no. 11, pp. 5906–5918, 2012.
- [15] J. Lorca Hernando and A. García Armada, "Piecewise Equalization of Zero Padding OFDM and FM-OFDM in Doubly-Dispersive Channels," in *2023 IEEE Globecom Workshops (GC Wkshps)*, 2023, pp. 811–817.
- [16] T. S. Rappaport, *Wireless communications*, 2nd ed. USA: Prentice Hall, 2002.
- [17] D. Tse and P. Viswanath, *Fundamentals of Wireless Communication*. USA: Cambridge University Press, 2005.
- [18] F. Hlawatsch and G. Matz, *Wireless Communications Over Rapidly Time-Varying Channels*. Academic Press, 2011.
- [19] O. Brandtsegg, S. Saue, and V. Lazzarini, "Live Convolution with Time-Varying Filters," *Applied Sciences*, vol. 8, no. 1, 2018. [Online]. Available: <https://www.mdpi.com/2076-3417/8/1/103>
- [20] J. C. Bowman and Z. Ghoggali, "The Partial Fast Fourier Transform," *Journal of Scientific Computing*, vol. 76, pp. 1578–1593, 2018.
- [21] Y. Li and L. Cimini, "Interchannel interference of OFDM in mobile radio channels," in *Globecom '00 - IEEE Global Telecommunications Conference. Conference Record (Cat. No.00CH37137)*, vol. 2, 2000, pp. 706–710 vol.2.
- [22] A. Garcia Armada, "Understanding the effects of phase noise in orthogonal frequency division multiplexing (OFDM)," *IEEE Transactions on Broadcasting*, vol. 47, no. 2, pp. 153–159, 2001.
- [23] A. Shahmansoori, G. E. Garcia, G. Destino, G. Seco-Granados, and H. Wymeersch, "5G Position and Orientation Estimation through Millimeter Wave MIMO," in *2015 IEEE Globecom Workshops (GC Wkshps)*, 2015, pp. 1–6.
- [24] H. Wymeersch and G. Seco-Granados, "Radio Localization and Sensing—Part II: State-of-the-Art and Challenges," *IEEE Communications Letters*, vol. 26, no. 12, pp. 2821–2825, 2022.
- [25] "3rd Generation Partnership Project; Technical Specification Group Radio Access Network; NR; Physical channels and modulation (Release 18)," 3GPP, Technical Specification 38.211 V18.4.0, 2024.
- [26] P. C. Hansen, "REGULARIZATION TOOLS: A Matlab package for analysis and solution of discrete ill-posed problems," *Numerical Algorithms*, vol. 6, p. 1–35, 1994.
- [27] Y. Jyotsna, N. Nithiyameenatchi, E. Konguvel, and M. Kannan, "Performance analysis of radix-2/3/5 decompositions in fixed point DIT FFT algorithms," in *2020 International Conference on Computer Communication and Informatics (ICCCI)*, 2020, pp. 1–7.
- [28] "3rd Generation Partnership Project; Technical Specification Group Radio Access Network; Study on channel model for frequency spectrum above 6 GHz (Release 14)," 3GPP, Technical Report TR 38.900 V14.2.0, 2017.
- [29] "3rd Generation Partnership Project; Technical Specification Group Radio Access Network; NR; User Equipment (UE) radio transmission and reception; Part 5: Satellite access Radio Frequency (RF) and performance requirements (Release 17)," 3GPP, Technical Specification 38.101-5 V17.3.0, 2023.
- [30] "Intelligent Transport Systems (ITS); Access Layer; Part 1: Channel Models for the 5.9 GHz frequency band," ETSI, Technical Report TR 103 257-1 V1.1.1, 2019.
- [31] "3rd Generation Partnership Project; Technical Specification Group Radio Access Network; Study on new radio access technology: Radio Frequency (RF) and co-existence aspects (Release 14)," 3GPP, Technical Report TR 38.803 V14.3.0, 2022.
- [32] R. Hadani, S. Rakib, S. Kons, M. Tsatsanis, A. Monk, C. Ibars, J. Delfeld, Y. Hebron, A. J. Goldsmith, A. F. Molisch, and R. Calderbank, "Orthogonal time frequency space modulation," 2018.
- [33] A. U. Ahmed, S. C. Thompson, D. W. Chi, and J. R. Zeidler, "Subcarrier based threshold performance enhancement in constant envelope ofdm," in *MILCOM 2012 - 2012 IEEE Military Communications Conference*, 2012, pp. 1–6.
- [34] A. U. Ahmed and J. R. Zeidler, "Novel Low-Complexity Receivers for Constant Envelope OFDM," *IEEE Trans. Signal Process.*, vol. 63, no. 17, pp. 4572–4582, 2015.
- [35] M. J. L. Morales, R. Dinis, and A. G. Armada, "Near-Optimal Detection of CE-OFDM Signals with High Power Efficiency via GAMP-based Receivers," in *2022 IEEE Globecom Workshops (GC Wkshps)*, 2022, pp. 7–12.
- [36] R. Bomfin, M. Chafii, A. Nimr, and G. Fettweis, "A robust baseband transceiver design for doubly-dispersive channels," *IEEE Transactions on Wireless Communications*, vol. 20, no. 8, pp. 4781–4796, 2021.
- [37] "3rd Generation Partnership Project; Technical Specification Group Radio Access Network; Solutions for NR to support non-terrestrial networks (NTN) (Release 16)," 3GPP, Technical Report 38.821 V16.2.0, 2023.
- [38] S. M. Kay, *Fundamentals of statistical signal processing: estimation theory*. USA: Prentice-Hall, Inc., 1993.
- [39] K. R. Patel and S. Dasrao Deshmukh, "2S (Superposition Coding, Successive Interference Cancellation) Operations in NOMA Technology for 5G Networks: Review and Implementation," in *2023 IEEE 8th International Conference for Convergence in Technology (I2CT)*, 2023, pp. 1–6.
- [40] X. Lai, Z. Chen, and Y. Zhao, "Basis expansion model for fast time-varying channel estimation in high mobility scenarios," in *Communications and Networking*, Q. Chen, W. Meng, and L. Zhao, Eds. Cham: Springer International Publishing, 2018, pp. 489–501.